

See discussions, stats, and author profiles for this publication at: <https://www.researchgate.net/publication/231643567>

# Mechanism of Selective Oxidation of Propene to Acrolein on Bismuth Molybdates from Quantum Mechanical Calculations

ARTICLE *in* THE JOURNAL OF PHYSICAL CHEMISTRY C · OCTOBER 2007

Impact Factor: 4.77 · DOI: 10.1021/jp074452a

CITATIONS

27

READS

75

## 5 AUTHORS, INCLUDING:



**Sanja Pudar**

California Institute of Technology

5 PUBLICATIONS 136 CITATIONS

SEE PROFILE



**Adri C.T. van Duin**

Pennsylvania State University

361 PUBLICATIONS 8,150 CITATIONS

SEE PROFILE



**William A. Goddard**

California Institute of Technology

1,333 PUBLICATIONS 68,233 CITATIONS

SEE PROFILE

# Mechanism of Selective Oxidation of Propene to Acrolein on Bismuth Molybdates from Quantum Mechanical Calculations

Sanja Pudar, Jonas Oxgaard, Kimberly Chenoweth, Adri C. T. van Duin, and William A. Goddard, III\*

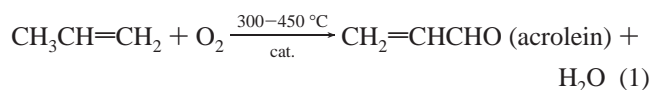
Materials and Process Simulation Center (139-74), California Institute of Technology, Pasadena, California 91125

Received: June 8, 2007; In Final Form: July 29, 2007

In order to provide a basis for understanding the fundamental chemical mechanisms underlying the selective oxidation of propene to acrolein by bismuth molybdates, we report quantum mechanical studies (at the DFT/B3LYP/LACVP\*\* level) of various reaction steps on bismuth oxide ( $\text{Bi}_4\text{O}_6/\text{Bi}_4\text{O}_7$ ) and molybdenum oxide ( $\text{Mo}_3\text{O}_9$ ) cluster models. For CH activation, we find a low-energy pathway on a  $\text{Bi}^{\text{V}}$  site with a calculated barrier of  $\Delta H^\ddagger = 11.0$  kcal/mol ( $\Delta G^\ddagger = 30.4$  kcal/mol), which is  $\sim 3$  kcal/mol lower than the experimentally measured barrier on a pure  $\text{Bi}_2\text{O}_3$  condensed phase. We find this process to be not feasible on  $\text{Bi}^{\text{III}}$  (it is highly endothermic,  $\Delta E = 50.9$  kcal/mol,  $\Delta G = 41.6$  kcal/mol) or on pure molybdenum oxide (prohibitively high barriers,  $\Delta E^\ddagger = 32.5$  kcal/mol,  $\Delta G^\ddagger = 48.1$  kcal/mol), suggesting that the CH activation event occurs on (rare)  $\text{Bi}^{\text{V}}$  sites on the  $\text{Bi}_2\text{O}_3$  surface. The expected low concentration of  $\text{Bi}^{\text{V}}$  could explain the 3 kcal/mol discrepancy between our calculated barrier and experiment. We present in detail the allyl oxidation mechanism over  $\text{Mo}_3\text{O}_9$ , which includes the adsorption of allyl to form the  $\pi$ -allyl and  $\sigma$ -allyl species, the second hydrogen abstraction to form acrolein, and acrolein desorption. The formation of  $\sigma$ -allyl intermediate is reversible, with forward  $\Delta E^\ddagger$  ( $\Delta G^\ddagger$ ) barriers of 2.7 (9.0 with respect to the  $\pi$ -allyl intermediate) kcal/mol and reverse barriers of 21.6 (23.7) kcal/mol. The second hydrogen abstraction is the rate-determining step for allyl conversion, with a calculated  $\Delta E^\ddagger = 35.6$  kcal/mol ( $\Delta G^\ddagger = 37.5$  kcal/mol). Finally, studies of acrolein desorption in presence of gaseous  $\text{O}_2$  suggest that the reoxidation significantly weakens the coordination of acrolein to the reduced  $\text{Mo}^{\text{IV}}$  site, helping drive desorption of acrolein from the surface.

## 1. Introduction

Catalytic oxidation of small olefins to unsaturated aldehydes and catalytic ammoxidation of small olefins to nitriles is of major commercial importance, representing 25% of the chemicals used in the manufacture of industrial and consumer products. In particular, about eight billion pounds of acrolein is produced annually,<sup>1</sup> primarily through catalytic oxidation of propene (eq 1)



In the early stages of this industry, acrolein was produced on simple bismuth and molybdenum oxide catalysts, but incorporation of other metals has significantly increased yield and selectivity. Even so, this process is still not optimal and even small improvements in the efficiency of the catalyst can have a major effect on environmental impact and energy requirements.

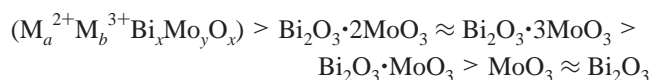
Due to the commercial importance of this process, many fundamental studies have been directed toward the understanding of the selective oxidation on Bi/Mo catalysts, yet there is still considerable uncertainty about the detailed chemical mechanisms involved. To gain more insight into this process and to lay a foundation for improving the catalysts, we have used quantum mechanical (QM) methods (at the DFT/B3LYP/

LACVP\*\* level) in conjunction with cluster models of the component oxides ( $\text{Bi}_2\text{O}_3$  and  $\text{MoO}_3$ ) to investigate the various steps involved in oxidizing propene to acrolein.

In our study we investigated the mechanism outlined in Scheme 1,<sup>2,3</sup> consisting of the following steps:

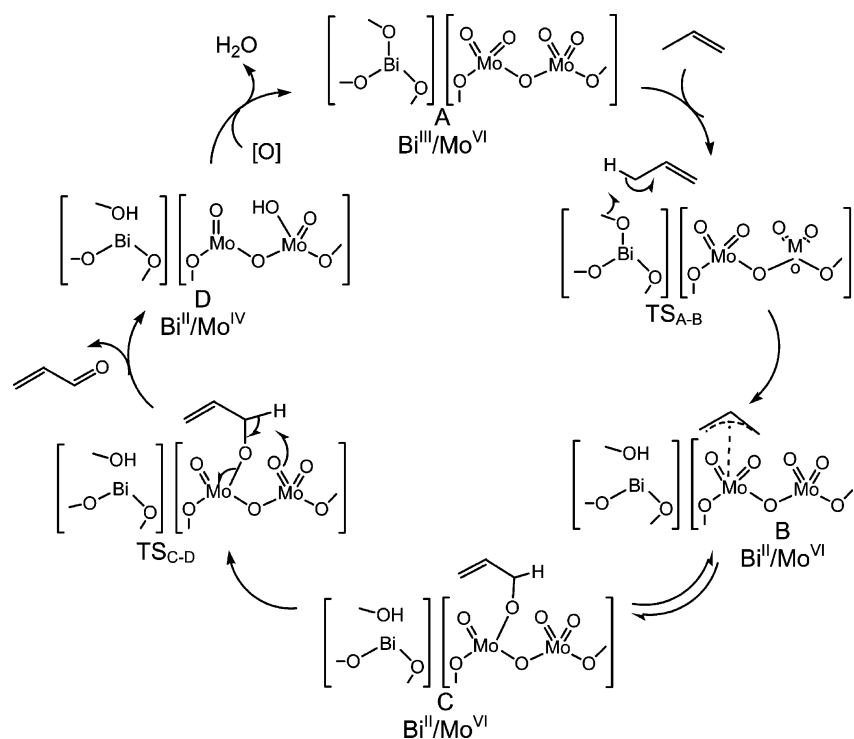
1. Propene coordination to the catalyst.
2. Allylic hydrogen abstraction by oxygen associated with bismuth ( $\text{TS}_{\text{A-B}}$  in Scheme 1) to form a  $\pi$ -allyl intermediate (B).
3. C–O bond formation on a molybdenum site to form a  $\sigma$ -allyl intermediate (C).
4. A second hydrogen abstraction on a molybdenum site ( $\text{TS}_{\text{C-D}}$ ) to form acrolein and a reduced Mo (D).
5. Reoxidation of the active site by lattice oxygen migration and filling of the vacancy by gaseous dioxygen.

**1.1. Overview of Experimental Work.** Experiments by Burrington and Grasselli<sup>4</sup> showed that at 320 °C, the rates of propene oxidation on Bi/Mo catalysts decrease in following order:



Pure  $\alpha\text{-Bi}_2\text{O}_3$  is found not to oxidize propene to acrolein but gives traces of 1,5-hexadiene,  $\text{CO}_2$ , and benzene. The 1,5-hexadiene is the expected product of allyl radical dimerization, suggesting that propene is activated on  $\alpha\text{-Bi}_2\text{O}_3$  but no further reaction occurs.<sup>4–7</sup> In addition, no oxidation occurs when

\* Corresponding author. E-mail: wag@wag.caltech.edu.

SCHEME 1: Proposed Mechanism for Propene Oxidation over Bismuth Molybdates<sup>a</sup><sup>a</sup> Refs 2 and 3.

propene is exposed to pure MoO<sub>3</sub>, most likely because MoO<sub>3</sub> is not capable of carrying out the first CH activation event. Burrington and Grasselli studied the reaction of MoO<sub>3</sub> with azopropene (which readily generates free allyl radicals) and reported a normalized acrolein yield of 51.5% (as well as 14.9% acetaldehyde, 14.7% CO<sub>2</sub>, 11.4% benzene, and 7.6% propene).<sup>4</sup> Somewhat contrary, Martir and Lunsford reported that if Bi<sub>2</sub>O<sub>3</sub> is placed upstream of MoO<sub>3</sub> in a flow reactor, only a small amount of acrolein is produced, and concluded that conversion of allyl radicals to acrolein is not very efficient over pure MoO<sub>3</sub>.<sup>8</sup> However, the difference in acrolein yields may be caused by the difference in experimental conditions and setup. In addition, the sequential placement of Bi<sub>2</sub>O<sub>3</sub> and MoO<sub>3</sub> reduced the amount of allyl radicals by a factor of 20, suggesting that MoO<sub>3</sub> acts as a radical scavenger.

Experimental studies also suggest that the rate-determining step is a  $\alpha$ -methyl hydrogen abstraction to form allylic radical intermediates. This was established from both the kinetic isotope effect (KIE) ( $k_H/k_D = 1.82$ ) and the isotopic distributions of oxygen insertion products from either allyl- or vinyl-D-labeled propenes.<sup>9–12</sup> Martir and Lunsford reported an activation energy of 14 kcal/mol for allyl radical formation over pure Bi<sub>2</sub>O<sub>3</sub>,<sup>8</sup> over the temperature range of 523–723 K. However, White and Hightower reported an activation energy of 22 kcal/mol for the catalytic reaction of propene and oxygen to form 1,5-hexadiene over Bi<sub>2</sub>O<sub>3</sub>,<sup>13</sup> whereas Swift et al. reported the value of 27.5 kcal/mol for cyclic reduction of Bi<sub>2</sub>O<sub>3</sub> by propene.<sup>6</sup> It is not clear why these reported values are so distinctly different, although it should be noted that the studies employ a wide range of experimental conditions. The experimental activation energy for  $\alpha$ -methyl hydrogen abstraction on mixed bismuth molybdates is seemingly less controversial and has been reported as 19–21 kcal/mol.<sup>2</sup>

Subsequent steps in the conversion of allyl intermediate to acrolein have been studied over molybdates using molecular probes, such as allyl alcohol, allyl amine, and selected D- and <sup>18</sup>O-labeled derivatives.<sup>4,14–17</sup> According to the observed isotopic

distributions of acrolein-3,3-*d*<sub>2</sub> and 1-*d*<sub>1</sub> in oxidation of either allyl alcohol-1,1-*d*<sub>2</sub> and -3,3-*d*<sub>2</sub>, or propene-1,1-*d*<sub>2</sub> and -3,3,3-*d*<sub>3</sub>, the initial rate-determining step results in the formation of a  $\pi$ -allyl intermediate, where allyl is  $\pi$ -bonded to a coordinately unsaturated Mo. This  $\pi$ -allyl species is rapidly and reversibly converted to a  $\sigma$ -allyl intermediate (the acrolein precursor) through the formation of a C–O bond, which is followed by the second hydrogen abstraction to give acrolein. The second hydrogen abstraction is the slow step in the conversion of the  $\sigma$ -allyl species to acrolein.

While it is clear that the first C–H activation event occurs on the bismuth and the subsequent oxidation occurs on the molybdenum, the difference between Martir and Lunsford's sequential Bi/Mo setup and the commercial mixed Bi/Mo catalysts (such as Bi<sub>2</sub>O<sub>3</sub>  $\times$  3MoO<sub>3</sub> and Bi<sub>2</sub>O<sub>3</sub>  $\times$  2MoO<sub>3</sub>) suggests that the functions of Bi<sub>2</sub>O<sub>3</sub> and MoO<sub>3</sub> are not merely additive.<sup>4</sup> The selectivity to acrolein of simple bismuth molybdates is about 90%, with only trace amounts of CO, CO<sub>2</sub>, and acetaldehyde being formed, which should be compared to the 51.5% acrolein yield of the pure MoO<sub>3</sub> reacting with allyl radicals.<sup>4</sup> The nature and cause of this nonadditive effect has not yet been explained.

**1.2. Earlier Theoretical Work.** Jang and Goddard previously studied the thermodynamics of propene activation by Bi<sup>III</sup> using a Bi<sub>4</sub>O<sub>6</sub> cluster model.<sup>18,19</sup> They found that the energy cost for the first hydrogen abstraction by oxygen is endothermic by 50.9 kcal/mol ( $\Delta G_{673K} = 41.6$  kcal/mol), possibly because it leads to Bi–O bond cleavage and produces a very unfavorable reduced Bi<sup>II</sup> state. These results appear contrary to the widely accepted view that the Bi<sup>III</sup> site is responsible for activation of propene.

Jang and Goddard also considered propene activation on a Bi<sup>V</sup> site using a Bi<sub>4</sub>O<sub>7</sub> cluster model, which has two different types of oxygens, bridging oxygens and terminal oxo oxygen. They found that the Bi<sup>V</sup> oxidized site leads to favorable C–H activation (due to favorable reduction of Bi<sup>V</sup> to Bi<sup>IV</sup>) with a reaction energy  $\Delta E = 6.4$  kcal/mol ( $\Delta G_{673K} = 2.5$  kcal/mol).

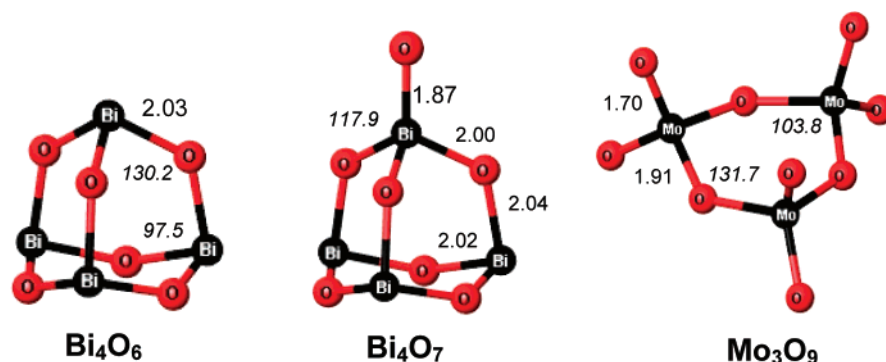


**Figure 1.** Cluster models used to represent the  $\text{Bi}^{\text{III}}$  site in  $\text{Bi}_4\text{O}_6$ , the  $\text{Bi}^{\text{V}}$  site in  $\text{Bi}_4\text{O}_7$ , and the  $\text{Mo}^{\text{VI}}$  site in  $\text{Mo}_3\text{O}_9$ . Selected bond lengths and angles are shown in angstroms and degrees, respectively.

In addition, they found that activating another propene at the  $\text{Bi}^{\text{IV}}$  site is exothermic with a  $\Delta E = -14.4$  kcal/mol ( $\Delta G_{673\text{K}} = -35.9$  kcal/mol). Indeed it is known that  $\text{Bi}_2\text{O}_3$  has the ability to chemisorb  $\text{O}_2$  dissociatively,<sup>20</sup> suggesting that in an oxidizing environment  $\text{O}_2$  reacts with surface  $\text{Bi}^{\text{III}}$  to form very small amounts of  $\text{Bi}^{\text{V}}$  species. However, Jang and Goddard calculated that the energy cost for formation of this  $\text{Bi}^{\text{V}}$  species by dissociative chemisorption of  $\text{O}_2$  molecule was high,  $\Delta E = 27.5$  kcal/mol ( $\Delta G_{673\text{K}} = 36.9$  kcal/mol). Since this energy includes half the dissociation energy of oxygen into atomic oxygens, Jang and Goddard suggested that this energy cost might be lowered significantly if the oxygen molecule dissociatively chemisorbs on some other site, such as  $\text{Fe}(\text{II})$ , and migrates to the bismuth site. Indeed, multicomponent catalysts that include Fe components show drastic improvement over simple bismuth molybdates, which was attributed mainly to improved activation of  $\text{O}_2$  to atomic lattice oxygen by the  $\text{Fe}(\text{II})/\text{Fe}(\text{III})$  redox couple.<sup>21</sup>

Jang and Goddard also studied the thermodynamics of the allyl adsorption on  $\text{Bi}^{\text{III}}$  and  $\text{Mo}^{\text{VI}}$  sites. They found that adsorption of allyl on  $\text{Bi}^{\text{III}}$  has a high energy cost ( $\Delta G_{673\text{K}} = 31.0$  kcal/mol), due formation of the unfavorable  $\text{Bi}^{\text{II}}$  state upon cleavage of the  $\text{Bi}-\text{O}$  bond. Thus the only plausible pathway over  $\text{Bi}_2\text{O}_3$  is the dimerization of allyl radicals. In contrast, chemisorption of allyl on the molybdenum terminal oxo sites is quite favorable ( $\Delta G_{673\text{K}} = 5.7$  kcal/mol). In addition, Jang and Goddard concluded that the second hydrogen abstraction step is most favorable when it occurs on a terminal oxo group of an adjacent molybdenum site.<sup>18,22</sup>

While Jang and Goddard's thermodynamic studies yielded significant insight into the chemistry of this process, they did not calculate the barriers for the various reaction steps, leaving uncertainties in their proposed mechanism. We now report the complete quantum mechanics based mechanism for propene oxidation on  $\text{Bi}_2\text{O}_3$  and  $\text{MoO}_3$ , including barriers. This report concentrates on cluster models of pure  $\text{Bi}_2\text{O}_3$  and  $\text{MoO}_3$ , without mixing of metals, in order to establish the fundamental mechanistic steps.

## 2. Technical Details

**2.1. Theoretical Methodology.** All calculations were performed using the B3LYP flavor of density functional theory (DFT), which combines exact HF exchange with the Becke generalized gradient exchange function<sup>23</sup> and the Lee, Yang, and Parr correlation functional (LYP).<sup>24</sup> Molybdenum and bismuth were described using the LACVP relativistic effective core potentials and basis sets of Hay and Wadt<sup>25</sup> which treat explicitly 14 valence electrons on molybdenum and 5 valence electrons on bismuth. The O, C, and H atoms were described using the Pople 6-31G\*\* basis set, including core and valence

electrons. Closed shell species were studied using RDFT, whereas UDFT was used for open shell species.

Geometries were fully optimized for each structure reported. The minima and saddle points were confirmed by diagonalizing the Hessian matrix and computing the vibrational frequencies. Each minimum had no imaginary frequencies, and each transition state was confirmed to be a first-order saddle point (one imaginary frequency). The vibrational frequencies were used to calculate zero-point energy (ZPE) and enthalpies at 0 K for each structure, as well as to calculate the enthalpy and entropy corrections to the QM energies at the experimental reaction temperature, 593 K. No frequency scaling term was used in calculating ZPE or thermodynamic properties. All calculations were carried out with the Jaguar 6.5 program.<sup>26</sup>

**2.2. Cluster Models.** In this work we explore C–H propene activation on pure bismuth and molybdenum oxide model cyclic clusters,  $\text{Bi}_4\text{O}_6$  and  $\text{Mo}_3\text{O}_9$ , respectively, as shown in Figure 1. The allyl conversion to acrolein was studied on a pure molybdenum oxide cyclic cluster model,  $\text{Mo}_3\text{O}_9$ . The cyclic cluster models were used to avoid having to terminate the clusters with OH species.

The crystal structure of  $\alpha\text{-Bi}_2\text{O}_3$  shows that each bismuth is connected to three nearest-neighbor oxygens, with each oxygen connected to two bismuth atoms.<sup>27</sup> Bismuth oxide vaporization experiments show that the gas phase consists of large amounts of closed shell  $(\text{Bi}_2\text{O}_3)_n$  clusters, including a neutral and stable  $\text{Bi}_4\text{O}_6$  species.<sup>28–30</sup> It has been proposed that  $\text{Bi}_4\text{O}_6$  has a compact cage structure with tricoordinated bismuth and bicoordinated oxygens.<sup>28,30</sup> Experiments on scattered bismuth oxide clusters  $(\text{Bi}_2\text{O}_3)_n\text{BiO}^+$  ( $1 \leq n \leq 4$ ) with ethene and propene show strong activity, suggesting that the isolated cluster has chemistry similar to that of bulk  $\text{Bi}_2\text{O}_3$ .<sup>31</sup> In addition, evidence of catalytic activity of  $\text{Bi}_4\text{O}_6^+$  toward alkenes via activation of molecular oxygen has been reported.<sup>32</sup> Thus, the cyclic  $\text{Bi}_4\text{O}_6$  cluster appears to mimic the chemistry and to retain the stoichiometry, neutrality, and coordination of bulk  $\text{Bi}_2\text{O}_3$ . Consequently we chose this cluster to represent the active site for propene activation (Figure 1). This cluster model has been used previously in theoretical studies of (amm)-oxidation of propene<sup>18,19</sup> and of bismuth oxide reactivity toward ethane and molecular oxygen.<sup>33</sup> For investigations of  $\text{Bi}^{\text{V}}$  we modified the  $\text{Bi}_4\text{O}_6$  to include an extra terminal oxygen on one Bi, resulting in a  $\text{Bi}^{\text{III}}_3\text{Bi}^{\text{V}}\text{O}_7$  cluster (abbreviated  $\text{Bi}_4\text{O}_7$ ). Since the number of  $\text{Bi}^{\text{V}}$  sites on the real surface should be low, this is a more realistic model than a “pure”  $\text{Bi}^{\text{V}}$  cluster, such as  $\text{Bi}^{\text{V}}_4\text{O}_{10}$ .

The crystal structure of  $\text{MoO}_3$  has two oxygen neighbors at an average distance of 1.68 Å ( $\text{Mo}=\text{O}$  oxo bonds), two oxygens at a distance of 2.02 Å ( $\text{Mo}-\text{O}-\text{Mo}$  bonds), and two oxygens at 2.3 Å (donor–acceptor bonds) as shown in Figure 2.<sup>34</sup> Thus,



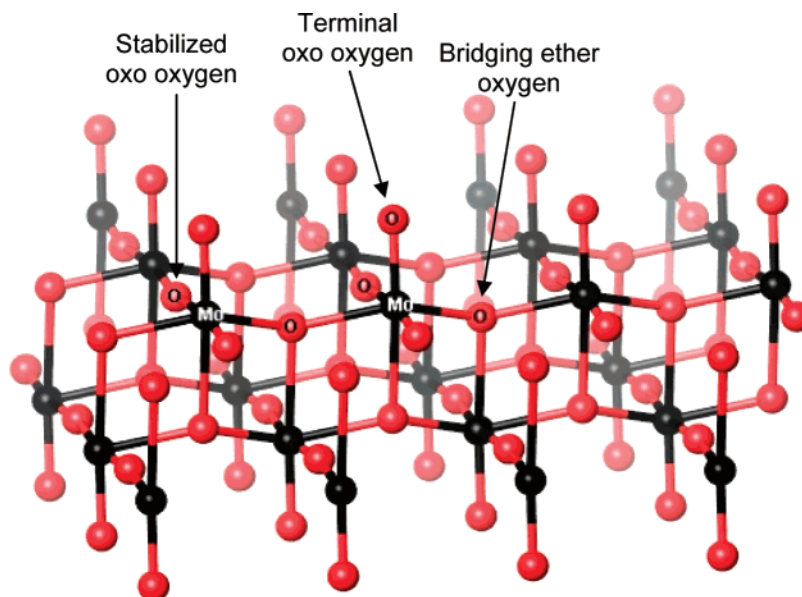


**Figure 2.** Types of oxygen atoms on the  $\alpha$ - $\text{MoO}_3(010)$  surface. The terminal and stabilized oxo oxygen distances to the bonded Mo are both 1.68 Å while the Mo–O–Mo ether-like single bonds are 2.02 Å.

this Mo is sometimes referred to as a distorted octahedron and sometimes as a distorted tetrahedron. Thus, there are three kinds of structurally different lattice oxygens in  $\text{MoO}_3$ : (1) *terminal oxo oxygen*, making an oxo bond to one molybdenum with a Mo–O distance of 1.68 Å, (2) *stabilized oxo oxygen*, making an oxo bond to one molybdenum with a Mo–O distance of 1.68 Å and weakly coupled in a donor–acceptor bond to another surface molybdenum at a distance of 2.30 Å, and (3) *ether bridging oxygen* atoms singly bonded to two surface molybdenum atoms at a distance of 2.02 Å, and weakly coupled in a donor–acceptor bond with a Mo of the underlying sublayer, at a distance of 2.31 Å. A similar bonding configuration is found in  $\alpha$ - $\text{Bi}_2\text{Mo}_3\text{O}_{12}$ , one of the most active mixed Mo/Bi catalysts.<sup>35</sup>

Evaporation of  $\text{MoO}_3$  samples from a Knudsen effusion source shows an abundance  $\text{Mo}_3\text{O}_9$  clusters in the vapor, which is proposed to have a six-membered ring structure as in Figure 1.<sup>36,37</sup> There have been several experiments on the reaction of these gas-phase molybdenum oxide clusters with small alcohols, alkanes, alkenes, and ammonia as a model study for mechanisms of heterogeneous catalysis.<sup>37,38</sup> These observations show that  $\text{Mo}_3\text{O}_9$  type clusters are reactive toward oxidation of CO, C–C activation of cyclopropane and propene, and dehydrogenation of  $\text{NH}_3$ . Thus, we chose the  $\text{Mo}_3\text{O}_9$  cluster to represent the active molybdenum site for oxidation (Figure 1). It has reactivity, stoichiometry, and coordination similar to that found in both pure  $\text{MoO}_3$  and  $\alpha$ - $\text{Bi}_2\text{Mo}_3\text{O}_{12}$  catalysts (see Figure 2). In this cluster model, each molybdenum is coordinated to two terminal oxo oxygens and two bridging or ether oxygens, corresponding to oxo and ether bridging oxygens in the  $\text{MoO}_3$  crystal. This cluster model was also used by Goddard and Jang in a mechanistic study of (amm)-oxidation of propene,<sup>18,19</sup> and by Fu et al. to study methane and propane activation.<sup>39,40</sup>

### 3. Results

Earlier work on this topic by Jang and Goddard explored the thermodynamics of various pathways, which we extend here to also include the relevant barriers. Propene activation is studied on bismuth and molybdenum oxides, and allyl intermediate conversion to acrolein on molybdenum oxide.

**3.1. Propene Activation. 3.1.1.  $\text{Bi}_4\text{O}_7$  Cluster.** As concluded from our previous work, we find that  $\text{Bi}^{\text{III}}$  is not able to activate

the allylic C–H bond of propene. Thus, we investigated the reactivity of the  $\text{Bi}^{\text{V}}$  toward propene activation. The potential energy surface (singlet spin state) for this process is shown in Figure 3. Here species **2** is propene weakly coordinating to a  $\text{Bi}^{\text{V}}$  oxo oxygen, with a  $\Delta E = -1.9$  kcal/mol ( $\Delta G_{593\text{K}} = 19.9$  kcal/mol). This low energy of coordination (indeed, endothermic on the free energy surface) agrees with the observation by Matsuura that propene adsorption on  $\text{Bi}_2\text{O}_3$  is weak compared to adsorption on  $\text{MoO}_3$  and  $\text{BiMoO}_6$ .<sup>41</sup> As shown in Figure 3, **2** features a methyl hydrogen coordinating to an oxo oxygen, with a H–O distance of 2.29 Å. Another isomer is found at  $\Delta E = -2.0$  kcal/mol ( $\Delta G = 22.2$  kcal/mol), where the hydrogen on the middle carbon coordinates to the oxo at distance of 2.23 Å.

The  $\Delta E^\ddagger$  of activation for the first hydrogen abstraction is 14.7 kcal/mol ( $\Delta G_{593\text{K}}^\ddagger = 30.4$  kcal/mol), with a transition state imaginary frequency of  $\nu = 665\text{i cm}^{-1}$  corresponding to the hydrogen abstraction by an oxo oxygen. In the transition state structure **TS1** (Figure 4) the Bi=O bond has increased from 1.87 to 2.07 Å, the methyl C–H bond has increased from 1.10 to 1.40 Å, and the O–H distance is decreased from 2.29 to 1.08 Å with respect to **2**. These bond distances indicate that the allyl radical is almost fully formed. However, the two C–C bonds are 1.45 and 1.35 Å, indicating that the allyl radical with its equivalent CC bond distances has not yet formed. Furthermore, the UDFT  $\langle S^2 \rangle$  value is 0.000, consistent with the closed shell character of this species, which is somewhat surprising since the product (**3**) is an uncoupled degenerate singlet/triplet. Thus, even though the radical is being formed, there is still significant HC bonding in **TS1**. To explore whether there is a surface crossing to the triplet state prior to forming **3**, we started with a structure similar to **TS1** but with a methyl–C–H–O angle close to 180°. This led to  $\langle S^2 \rangle$  value of 0.700 and a large vibrational imaginary frequency corresponding to methyl–H abstraction by terminal oxygen. Optimization of the transition state led to a structure with a methyl–C–H–O angle of 155° and  $\langle S^2 \rangle = 0.093$ , suggesting that the effect of any possible spin crossing is insignificant to the relevant chemistry, and we thus did not investigate this further.

Propene activation on  $\text{Bi}_4\text{O}_7$  leads to the products  $\text{Bi}_4\text{O}_7\text{H}$  (**3**) and an allyl radical, with a relative energy of  $\Delta E = 4.1$

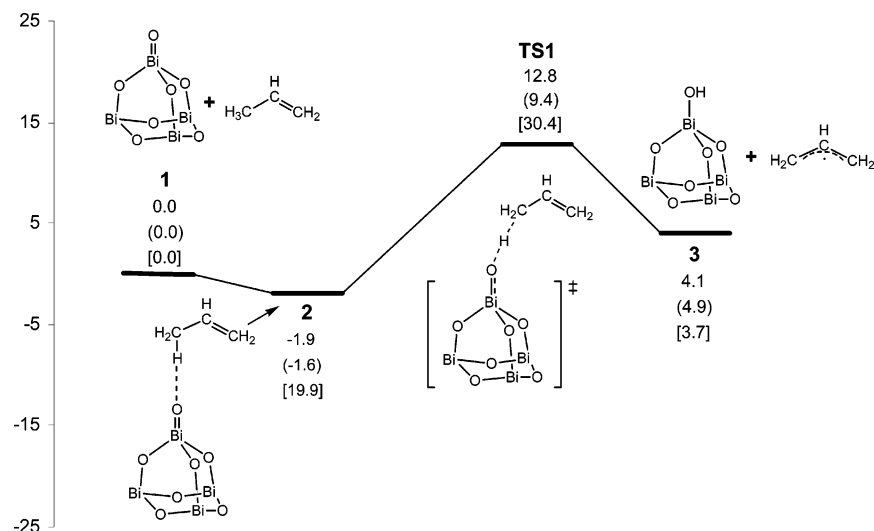


**Figure 3.** Singlet potential energy surface for C–H propene activation on  $\text{Bi}_4\text{O}_7$ . The  $\text{Bi}^{\text{V}}$  site readily activates propene, with a  $\Delta H_{\text{OK}}$  barrier of 11.0 kcal/mol, just 3.0 kcal/mol lower than the  $\Delta H^\ddagger$  observed for allyl radical formation on  $\text{Bi}_2\text{O}_3$ . The top energy is the  $\Delta E$  from QM, the middle is  $\Delta H_{\text{OK}} = \Delta E + \Delta \text{ZPE}$ , and the bottom is  $\Delta G_{593\text{K}}$ . All reported values are in kcal/mol.

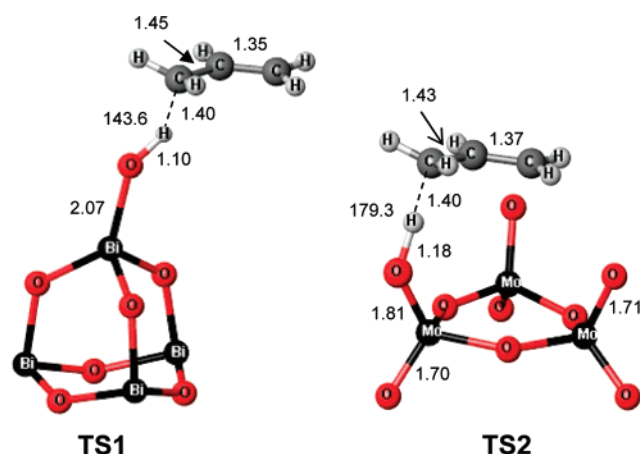


**Figure 4.** Structural parameters for the transition states of C–H propene activation on  $\text{Bi}_4\text{O}_7$  (**TS1**) and  $\text{Mo}_3\text{O}_9$  (**TS2**). Bonds lengths are shown in angstroms.

kcal/mol ( $\Delta G_{593\text{K}} = 3.7$  kcal/mol). In species **3**, the  $\text{Bi}^{\text{V}}$  center is reduced to  $\text{Bi}^{\text{IV}}$ , with a spin density of  $0.759 e^-$  located in a bismuth  $s$  orbital and an oxygen  $p$  orbital positioned along the  $\text{Bi}^{\text{IV}}\text{--O}$  bond. The  $\text{Bi}^{\text{IV}}\text{--O}$  bond length is  $2.15 \text{ \AA}$ , while the other  $\text{Bi}^{\text{III}}\text{--O}$  bonds have an average bond length of  $2.04 \text{ \AA}$ . The spin density and elongated  $\text{Bi}\text{--O}$  distance at the reduced  $\text{Bi}$  site indicate that the  $\text{Bi}\text{--O}$  bond order is about 0.5, which may assist the activation of another propene on this site to produce  $\text{H}_2\text{O}$ ,  $\text{Bi}_4\text{O}_6$ , and a second allyl radical. In fact, we found that activation of propene on  $\text{Bi}_4\text{O}_7\text{H}$  (**3**) is highly exothermic ( $\Delta E = -14.4$  kcal/mol,  $\Delta G_{673\text{K}} = -35.9$  kcal/mol).<sup>18</sup> The fast consumption and restoration of  $\text{Bi}^{\text{V}}$  species to  $\text{Bi}^{\text{III}}$  upon reacting with another propene may explain the lack of spectroscopic evidence for the existence of  $\text{Bi}^{\text{V}}$  on  $\text{Bi}_2\text{O}_3$  or bismuth molybdate catalysts.

**3.1.2.  $\text{Mo}_3\text{O}_9$  Cluster.** We also investigated propene activation on  $\text{Mo}^{\text{VI}}$  (using the  $\text{Mo}_3\text{O}_9$  cluster model) to understand the experimentally observed inability of  $\text{MoO}_3$  to generate allyl radicals. The singlet potential energy surface for this process is shown in Figure 5. Species **5** represents the coordination of propene to molybdenum, where propene is positioned over and parallel to the  $\text{Mo}_3\text{O}_9$  ring at the distance of  $\sim 3 \text{ \AA}$ , with no measurable interaction between the propene  $\pi$  electrons and

molybdenum. This weakly bound interaction has a  $\Delta E = -5.1$  kcal/mol ( $\Delta G_{593\text{K}} = 14.8$  kcal/mol).

We also found another coordination isomer with  $\Delta E = -5.9$  kcal/mol ( $\Delta G_{593\text{K}} = 17.9$  kcal/mol) in which the propene acts as a  $\pi$ -donor to the acidic open site of the  $\text{Mo}$  cluster at a distance of  $\sim 2.8 \text{ \AA}$ . Since this case has the propene positioned on the side of the ring, we do not expect this structure to exhibit low-energy barriers and we consider it a less realistic mimic of the actual  $\text{MoO}_3$  surface.

We calculate that  $\Delta E^\ddagger = 32.5$  kcal/mol for the  $\alpha$ -methyl hydrogen abstraction by a terminal oxygen through **TS2**, which is considerably higher than the cost for the same process on  $\text{Bi}^{\text{V}}$  site. Furthermore, there is a significant entropic cost of associating the propene with the surface (at 593 K, the coordination of propene to  $\text{Mo}_3\text{O}_9$  in **5** is uphill by  $\Delta G_{593\text{K}} = 14.8$  kcal/mol). This leads to a net  $\Delta G_{593\text{K}}^\ddagger = 48.1$  kcal/mol, which is prohibitively high even at  $320^\circ\text{C}$ . This agrees with the experimentally observed inactivity of  $\text{MoO}_3$  toward propene.<sup>4</sup>

The imaginary normal mode for transition state **TS2** corresponds to hydrogen abstraction by the terminal oxo group, with a vibrational frequency  $\nu = 1699i \text{ cm}^{-1}$ . In **TS2** (see Figure 4) the  $\text{O}\text{--H}$  bond is almost formed ( $\text{O}\text{--H} = 1.18 \text{ \AA}$ ), the  $\text{C}\text{--H}$  bond is broken ( $\text{C}\text{--H} = 1.40 \text{ \AA}$ ), and the  $\text{Mo}\text{=O}$  bond is elongated from  $1.70$  to  $1.81 \text{ \AA}$ , corresponding to a reduction in bond order from 2 to 1.5. Here, the two  $\text{C}\text{--C}$  bonds of the allylic portion of **TS2** are nearly equal ( $1.43$  and  $1.37 \text{ \AA}$ ), which can be compared to the  $\text{C}\text{--C}$  bonds in propene of  $1.50$  and  $1.33 \text{ \AA}$ . The  $\langle S^2 \rangle$  value of  $0.633$  indicates open shell character, with the spin density located in the allyl  $\pi^*$  orbital and the molybdenum  $d_{zx}$  orbital (lying in the plane of the  $\text{Mo}_3\text{O}_9$  ring). This is nearly identical to the spin population in intermediate **6**, which represents coordination of allyl radical to  $\text{Mo}_3\text{O}_9\text{H}$ . This analysis suggests that the allyl radical is almost fully formed in **TS2**.

The product of the first hydrogen abstraction has the allyl radical positioned on top and parallel to the  $\text{Mo}_3\text{O}_9\text{H}$  ring (**6**), which is uphill by  $21.6$  kcal/mol ( $\Delta G_{593\text{K}} = 40.8$  kcal/mol). The  $\langle S^2 \rangle$  value is  $0.991$ , indicating an uncoupled diradicaloid singlet, with the spin density located on the allyl  $\pi^*$  and the molybdenum  $d_{zx}$  orbitals, the same as found for the propene activation transition state **TS2**. Thus, the reason for the high

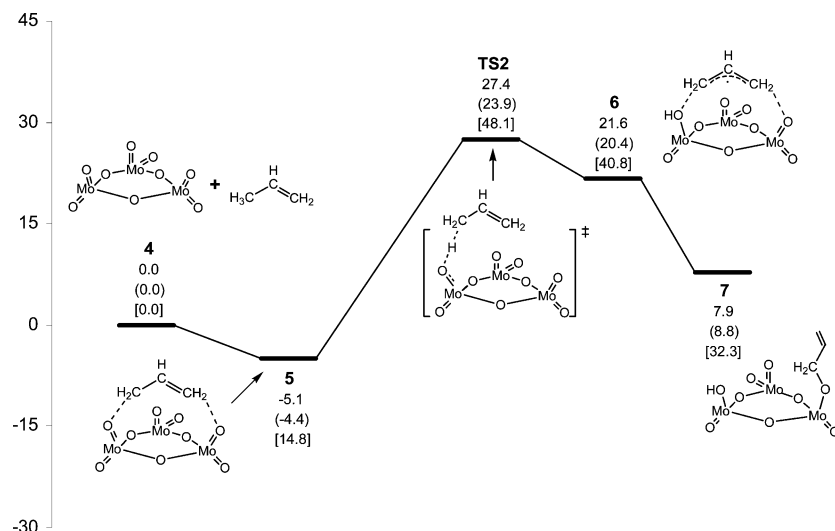


**Figure 5.** Singlet potential energy surface for C–H propene activation and subsequent allyl adsorption on Mo<sub>3</sub>O<sub>9</sub>. The high net  $\Delta G_{593\text{K}}$  barrier renders MoO<sub>3</sub> inactive for propene oxidation. The top energy is the QM  $\Delta E$ , the middle value is  $\Delta H_{0\text{K}} = \Delta E + \Delta \text{ZPE}$ , and the bottom one is  $\Delta G_{593\text{K}}$ . All reported values are in kcal/mol.

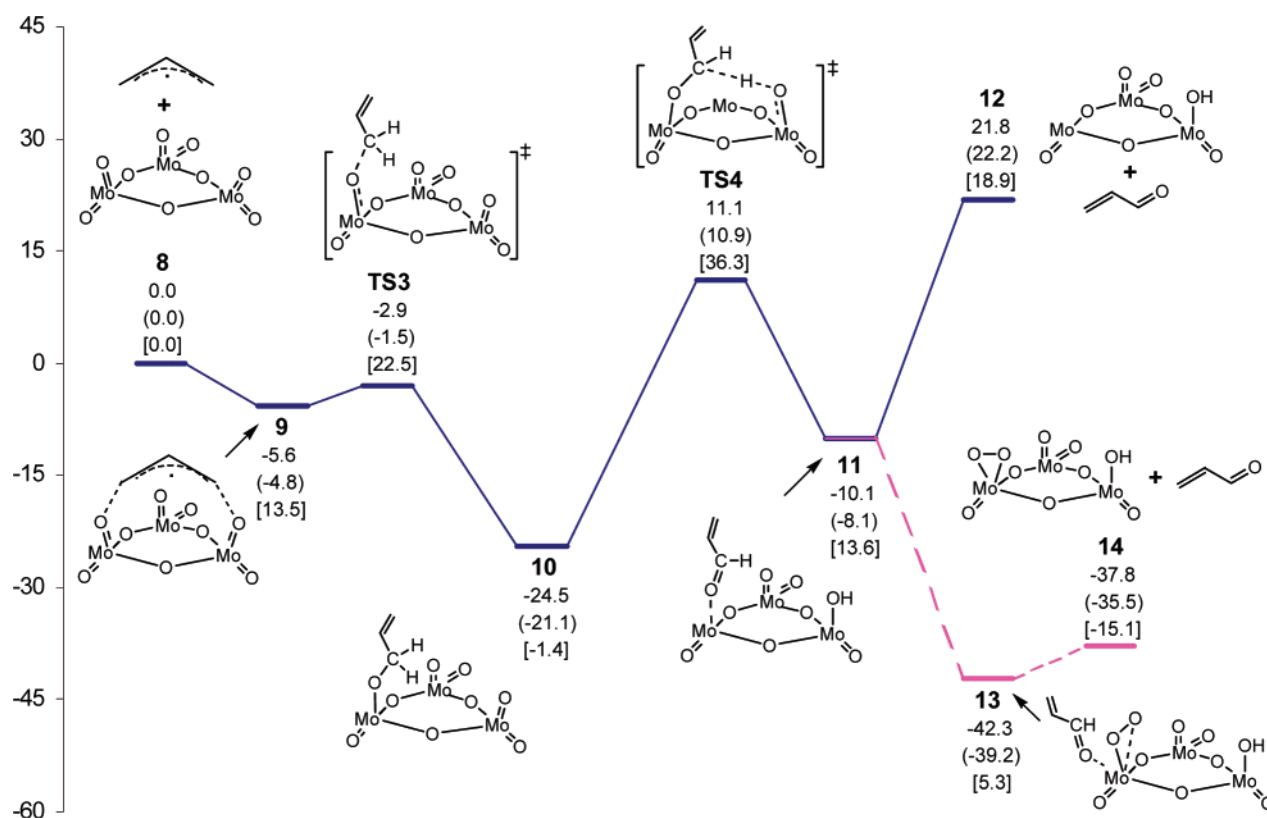


**Figure 6.** Potential energy surface for conversion of allyl to acrolein on Mo<sub>3</sub>O<sub>9</sub> cluster (all states of spin doublets). The solid line represents the mechanism in absence of O<sub>2</sub>, while the dashed line represents the O<sub>2</sub>-assisted acrolein desorption. The net  $\Delta G_{593\text{K}}$  barrier of 37.5 kcal/mol suggests that MoO<sub>3</sub> is capable of allyl oxidation, but with lower activity than bismuth molybdates. The top energy is the  $\Delta E$  from QM, the middle one is  $\Delta H_{0\text{K}} = \Delta E + \Delta \text{ZPE}$ , and the bottom one is  $\Delta G_{593\text{K}}$ . All reported values are in kcal/mol.

barrier for C–H activation on pure MoO<sub>3</sub> is the instability of the allyl + MoO<sub>2</sub>OH intermediate.

Trapping of the allyl radical by a neighboring Mo=O group of Mo<sub>3</sub>O<sub>9</sub>H to form the open shell singlet Mo<sub>3</sub>O<sub>7</sub>(OCH<sub>2</sub>CHCH<sub>2</sub>)(OH) **7**, with  $\langle S^2 \rangle = 0.725$ , is exothermic by 13.7 kcal/mol ( $\Delta G_{593\text{K}} = -8.5$  kcal/mol) with respect to **6**. Although this does not improve the kinetics of the CH activation, it is consistent with the experimental observation that MoO<sub>3</sub> is an effective radical scavenger.<sup>8</sup> The triplet state for this species is 2.2 kcal/mol higher than its respective open shell singlet,

suggesting that there is some electronic coupling between the spins in **7**, albeit only a few kilocalories per mole.

**3.2. Allyl Oxidation.** The allyl radical formed on the bismuth oxide is expected to transfer to the molybdenum oxide before further conversion to acrolein. To study this process, we used the Mo<sub>3</sub>O<sub>9</sub> cluster model with a pregenerated allyl radical. The potential energy surface for this process is shown in Figure 6, while the structural parameters for important intermediates and transition states are shown in Figure 7. Overall, the conversion of one allyl radical to acrolein is endothermic, with  $\Delta E = 21.8$

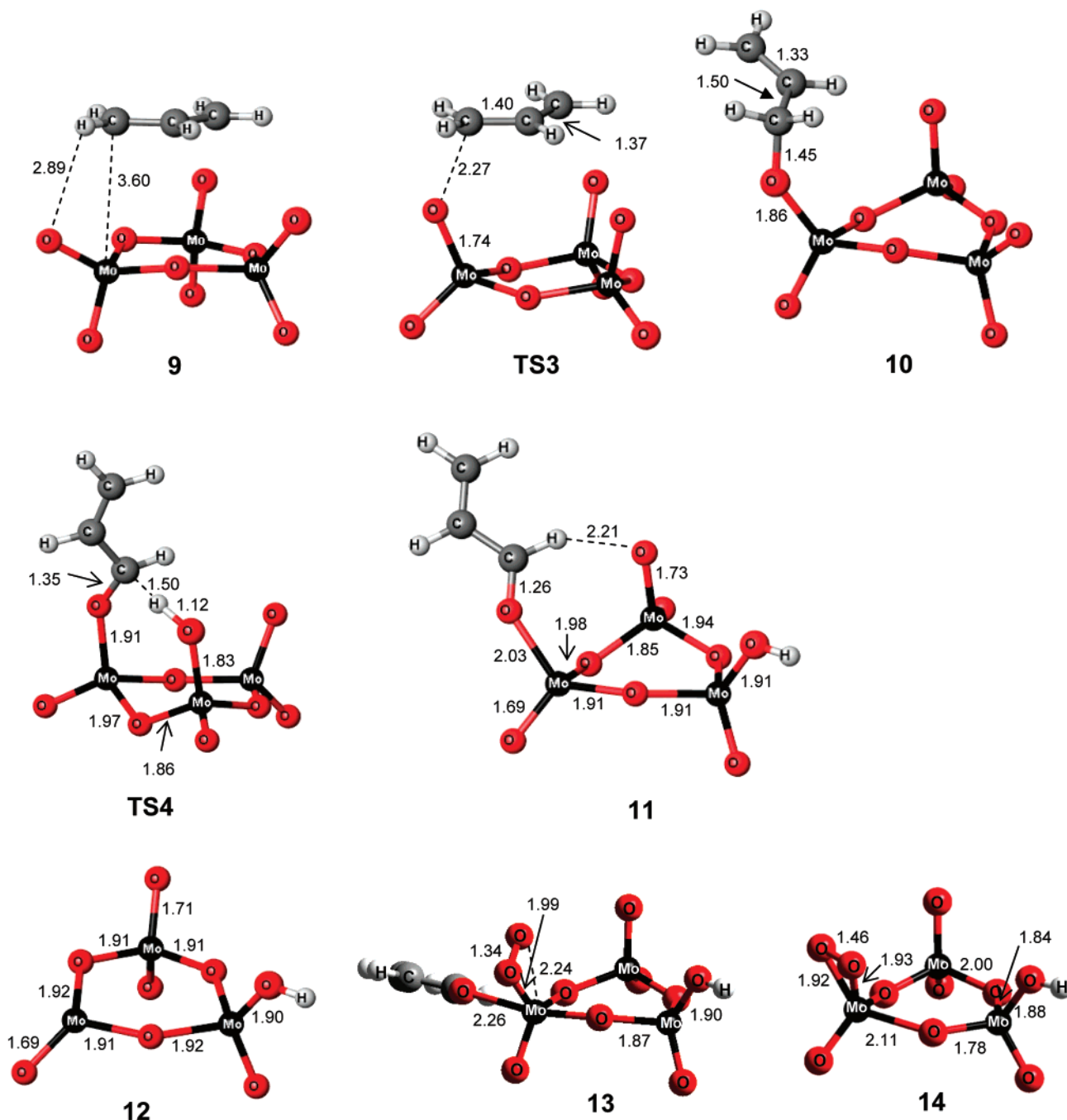


**Figure 7.** Structural parameters for the intermediates and transition states of the allyl oxidation on  $\text{Mo}_3\text{O}_9$ . Bond distances are shown in angstroms.

kcal/mol ( $\Delta G_{593\text{K}} = 18.9$  kcal/mol). However, by including the energy of  $\text{O}_2$  reoxidation, the overall reaction energy becomes  $\Delta E = -37.8$  kcal/mol ( $\Delta G_{593\text{K}} = -15.1$  kcal/mol), suggesting that the reoxidation is important for driving the overall reactivity.

**3.2.1. Allyl Physisorption:  $\pi$ -Allyl.** The first step is the coordination of the allyl radical to  $\text{Mo}_3\text{O}_9$  (**8**) to form the  $\pi$ -allyl intermediate **9**, with  $\Delta E = -5.6$  kcal/mol ( $\Delta G_{593\text{K}} = 13.5$  kcal/mol). Intermediate **9** has the allyl positioned directly over and parallel to the  $\text{Mo}_3\text{O}_9$  ring, with the allylic hydrogens at approximately 2.80 Å from terminal oxygens.

Another coordination isomer was found with a  $\Delta E = -5.9$  kcal/mol ( $\Delta G_{593\text{K}} = 16.8$  kcal/mol) in which the allyl is positioned at the side of the ring and interacting directly with the acidic site (empty coordination site) of one molybdenum atom at 2.85 Å. However, we do not expect this to lead to more favorable transition states and did not pursue this coordination

further. Again, the reactivity of  $\text{Mo}_3\text{O}_9$  toward allyl is consistent with the observed role of molybdenum oxide as an effective allyl radical scavenger.

**3.2.2. Allyl Chemisorption:  $\sigma$ -Allyl.** The  $\pi$ -allyl intermediate can convert to the  $\sigma$ -allyl intermediate **10** through a C–O bonding transition state, **TS3**, with a barrier of  $\Delta E^\ddagger = 2.7$  kcal/mol ( $\Delta G_{593\text{K}}^\ddagger = 9.0$  kcal/mol with respect to **9**, 22.5 kcal/mol with respect to **8**). In **TS3**, the Mo–O distance at the allyl adsorption site is 1.74 Å, whereas the C–O distance is 2.27 Å, indicating an early transition state. The transition state eigenvector has the character of C–O bond formation (with an imaginary frequency of  $\nu = 169.4i$   $\text{cm}^{-1}$ ). Since the  $\Delta G_{593\text{K}}$  barrier for formation of  $\sigma$ -allyl species starting from **9** is only 9.0 kcal/mol, this process should be very rapid, as observed experimentally.<sup>14</sup>



The  $\sigma$ -allyl product, **10**, has a  $\Delta E = -18.9$  kcal/mol ( $\Delta G_{593K} = -14.9$  kcal/mol) with respect to **9**. The C–O bond distance in **10** is 1.46 Å (compare to 1.41 for a normal CO bond as in methanol), and the activated Mo<sup>V</sup>–O bond distance is 1.86 Å (a bond order of  $\sim 1.5$ ). The  $\langle S^2 \rangle = 0.756$ , consistent with a doublet, with the spin density located in the molybdenum  $d_{zx}$  orbital, lying in the plane of Mo<sub>3</sub>O<sub>9</sub> ring. A second  $\sigma$ -allyl conformer, with  $\Delta E = -20.9$  kcal/mol ( $\Delta G_{593K} = -11.1$  kcal/mol) with respect to **9**, was located as well. In this structure, the allyl is positioned exactly on the top of the Mo<sub>3</sub>O<sub>9</sub> ring, which prevents it from participating in allyl conversion unless it rotates to yield the first conformer, **10**. Although this conformer is the ground state for **10**, we do not expect this to have any chemical significance.

The reverse process (i.e., the back-conversion of the  $\sigma$ -allyl to the  $\pi$ -allyl species) has a barrier of 21.6 kcal/mol ( $\Delta G_{593K}^\ddagger = 23.9$  kcal/mol). Thus **9**  $\rightarrow$  **10** should be reversible under reaction conditions. This is in the agreement with experiments, which show a rapid equilibrium between the  $\pi$ -allyl and the  $\sigma$ -allyl species.<sup>14</sup> However, we find **9** and **10** do not have equal energies (as postulated by Grasselli and Burrington).<sup>17</sup> The formation of the  $\sigma$ -allyl is more favorable than the  $\pi$ -allyl due to the energy gained from C–O bond formation, as compared to the weak interaction in  $\pi$ -allylic intermediate.

**3.2.3. Hydrogen Abstraction.** The next step in the allyl oxidation is a second hydrogen abstraction from **10** to yield **11** with a Mo<sup>V</sup>–OH site and acrolein coordinated to a reduced Mo<sup>IV</sup>. This occurs through a seven-membered transition state structure, **TS4**, with a calculated barrier of  $\Delta E^\ddagger = 35.6$  kcal/mol ( $\Delta G_{593K}^\ddagger = 37.7$  kcal/mol). The transition state eigenvector represents the hydrogen abstraction by a neighboring terminal Mo=O group (with an imaginary frequency of  $\nu = 1070i$  cm<sup>-1</sup>). The O–H distance in the forming bond is 1.08 Å, while the  $\alpha$ -C–H distance has increased from 1.09 Å in **10** to 1.64 Å, and the C–O bond distance decreased from 1.46 to 1.35 Å. These bond distances indicate that the hydrogen abstraction is almost complete in **TS4**. Furthermore, the Mo=O bond at the acrolein formation site elongates from 1.86 to 1.92 Å while the Mo=O bond at the hydrogen accepting site elongates from 1.71 to 1.83 Å, consistent with the transformation of a Mo–O  $\sigma$ -bond to a Mo  $\leftarrow$  O coordination and of a Mo=O  $\pi$ -bond to a Mo–O  $\sigma$ -bond. The distance between the two reduced Mo atoms decreases from 3.60 to 3.36 Å, indicating a strong interaction between the two metal centers and possibly spin coupling. The  $\langle S^2 \rangle$  value is 0.764, with the unpaired spin localized on the  $d_{yx}$  orbital of the Mo<sup>IV</sup> atom.

Since the product, **11**, has one Mo<sup>V</sup> center (spin doublet) and one Mo<sup>IV</sup> center (spin triplet), we expect the ground state to be a quartet. Indeed, a second transition state (**TS4'**) was found that has a slightly lower energy ( $\Delta E^\ddagger = 33.5$  kcal/mol,  $\Delta G_{593K}^\ddagger = 34.0$  kcal/mol), with a significant amount of spin contamination ( $\langle S^2 \rangle = 0.989$ ). The structure of this transition state is very similar to that of the **TS4** doublet, except that the O–H bond distance is 1.15 Å, the  $\alpha$ -C–H distance is 1.46 Å, and the C–O distance is 1.38 Å, indicating that the O–H is not as close to being formed as in the **TS4** doublet. The spin density is located on the  $d_{yx}$  orbitals of the *two* reduced molybdenum atoms, as well as on the  $\pi^*$  orbital of acrolein moiety. This spin contamination suggests a low-energy quartet state, and we sought to isolate the pure quartet analogue of **TS4**, without success. Scanning of quartet potential energy surface along the forming O–H and breaking Mo=O bonds resulted in monotonic decreases in energy, where several selected points along this path have only small imaginary frequencies (less than 80i cm<sup>-1</sup>)

corresponding to the second hydrogen abstraction. In addition, optimization of **TS4** on the quartet surface with constrained C–H and O–H distances yielded a geometry with an imaginary frequency of 18i cm<sup>-1</sup>. Consequently, it is not clear whether the lower energy of the contaminated **TS4'** is due to artificial stabilization or whether it is a true low-energy transition state. Fortunately, the difference between **TS4** and **TS4'** of  $-2.1$  kcal/mol ( $\Delta \Delta G_{593K} = -3.9$  kcal/mol) does not significantly influence our mechanistic analysis.

The experimental  $k_H/k_D$  ratio is  $\approx 2.5$  at 320 °C for the second hydrogen abstraction (obtained from molecular probe experiments using alcohol-1,1- $d_2$  and -3,3- $d_2$ ).<sup>14</sup> Our calculations lead to  $k_H/k_D = 2.54$  (no tunneling corrections) using the doublet **TS4** structure, which agrees with experiment. However, our calculated KIE for **TS4'** is also 2.54, which prevents us from distinguishing the correct transition state based on KIEs. However, we expect that the transition to the spin quartet state would have little effect on the chemistry, and henceforth we will use **TS4** in our discussions on this chemistry.

Comparing the net  $\Delta G_{593K}$  barriers for the second hydrogen abstraction (37.7 kcal/mol) and propene activation on Mo<sub>3</sub>O<sub>9</sub> (48.1 kcal/mol), we conclude that the first process is plausible at the temperature of 320 °C, whereas the second is not. Consequently, MoO<sub>3</sub> should be capable of oxidizing allyl into acrolein, but it is not capable of activating propene. Furthermore, the barrier of 37.7 kcal/mol is quite high, which is in good agreement with experiments showing that allyl oxidation over MoO<sub>3</sub> at 320 °C yields between trace and 51.5% of acrolein, depending on the experimental setup.<sup>4,8</sup> This suggests that the conversion of allyl to acrolein is not particularly efficient over pure MoO<sub>3</sub>.

**TS4** (as well as **TS4'**) leads to intermediate **11**, which resembles acrolein coordinated to the reduced Mo<sup>IV</sup> site. The C=O bond distance in **11** is 1.26 Å, which compares to 1.22 Å in isolated acrolein. Furthermore, the Mo  $\leftarrow$  O distance is 2.03 Å, suggesting that this acrolein precursor is still strongly coordinated to Mo site. In addition, the remaining Mo=O bond at the acrolein formation site is 0.02 Å shorter than the Mo=O in the nonreduced cluster Mo<sub>3</sub>O<sub>9</sub>, consistent with a stabilization effect of a spectator oxo group through the formation of a partial triple Mo–O bond, as discovered by Allison and Goddard<sup>22</sup> and Rappe and Goddard<sup>42</sup> in earlier studies on these and related systems. The  $\langle S^2 \rangle$  value is 0.878, with the majority of the spin density located in the  $d_{xz}$  orbital on the Mo<sup>V</sup> atom, but with the remaining density found in the  $d_{xy}$  and  $d_{x^2-y^2}$  orbitals of Mo<sup>IV</sup>. This is consistent with our calculations showing that the lowest spin state for the reduced Mo<sub>3</sub>O<sub>8</sub> species has one Mo<sup>IV</sup> and two Mo<sup>VI</sup> centers, leading to the spin triplet expected for a  $d^2$  metal with tetrahedral coordination (the open shell singlet is 5.9 kcal/mol higher in energy). Therefore, all species leading to a combination of Mo<sup>IV</sup> and Mo<sup>V</sup> sites are bound to suffer from spin contamination, as the quartet states become more stable. In these quartet states, two electrons are located in the  $d_{xy}$  and  $d_{x^2-y^2}$  orbitals of the Mo<sup>IV</sup> center, and the third electron is located in the  $d_{xz}$  orbital on the Mo<sup>IV</sup> center.

**3.2.4. Acrolein Desorption.** The desorption of acrolein (dashed line in Figure 6) results in the reduced Mo<sub>3</sub>O<sub>8</sub>H species **12**, with a desorption energy  $\Delta E = 31.9$  kcal/mol ( $\Delta G_{593K} = 5.3$  kcal/mol), indicating a very strong binding to the reduced Mo<sup>IV</sup> site. We could find no additional barrier for this desorption, and optimization of Mo<sub>3</sub>O<sub>8</sub>H and acrolein initially placed at a distance of 5.0 Å resulted in formation of **11** with monotonic decrease in energy. The  $\langle S^2 \rangle$  value for **12** is 1.426, indicating strong spin contamination due to a quartet state that is 4.8 kcal/

mol ( $\Delta\Delta G_{593K} = -5.6$  kcal/mol) lower in energy than the doublet state. The spin density of **12** is located in the  $d_{xz}$  orbital on the  $\text{Mo}^{\text{V}}$  site, and in the  $d_{xy}$  and  $d_{x^2-y^2}$  orbitals on the  $\text{Mo}^{\text{IV}}$  site, where one spin is up and one spin is down. A similar spin density is present in the quartet state of **12**, except that both spins on  $\text{Mo}^{\text{IV}}$  are up, giving rise to the  $m_s = 3/2$  state. A lower energy isomer of **12** was found (desorption  $\Delta E = 28.8$  kcal/mol,  $\Delta G_{593K} = 7.7$  kcal/mol) where the OH group is bridging the two reduced molybdenum atoms; however, this structure involves the contraction of Mo–Mo distance from 3.67 to 3.12 Å. However, in a larger crystal we expect this contraction to be associated with a large energetic penalty, as this would cause a distortion of the solid-state structure. Consequently, we believe the lower energy of this intermediate to be an artifact of the model cluster used in this study and we did not use this structure for further analysis.

Species **12** has two reduced molybdenum sites, one vacant  $\text{Mo}^{\text{IV}}$  site and one  $\text{Mo}^{\text{V}}\text{--OH}$  site, which probably contributes substantially to the calculated endothermicity of the process. Indeed, acrolein is expected to bind more strongly to  $\text{Mo}^{\text{IV}}$  than to  $\text{Mo}^{\text{VI}}$ , and analysis of the bridging  $\text{Mo}^{\text{IV}}\text{--O}$  single bonds shows that they contract as acrolein leaves, compensating for the loss of electron density. We suspect that this process is far more effective in the  $\text{MoO}_3$  crystal, where, in addition to bridging ether oxygens, there are *stabilized oxo* oxygens by neighboring acidic Mo sites ( $r_{\text{Mo--O}} = 2.30$  Å), plus ether oxygens in the second layer directly below the molybdenum atoms of the surface layer (see the  $\text{MoO}_3$  crystal in Figure 2). Indeed, it is possible that the surface  $\text{Mo}^{\text{IV}}$  might be reoxidized by adjacent lattice oxygens as the acrolein is desorbed, a process that strongly resembles the suggested mechanism for reoxidation of the reduced sites.<sup>43–45</sup>

**3.2.5. Dioxygen-Assisted Acrolein Desorption.** To further understand how reoxidation can affect acrolein desorption, we considered the energetics for  $\text{O}_2$ -assisted desorption of acrolein. A similar mechanism was proposed recently for oxidative dehydrogenation of propane conversion to propene over the cyclic  $\text{V}_4\text{O}_{10}$  cluster by Cheng et al.<sup>46</sup> This has also been applied in a recent study of  $\text{CH}_4$  activation on Si-supported  $\text{Mo=O}$  by Chempath and Bell.<sup>47</sup> Although it is generally assumed that dioxygen dissociates at a site different from the catalytically active site, we considered the consequence of allowing an  $\text{O}_2$  to coordinate with the reduced  $\text{Mo}^{\text{IV}}$  site in **11** (prior to desorption of acrolein).

We find that the coordination of  $\text{O}_2$  promotes acrolein desorption quite significantly, destabilizing the binding of acrolein and avoiding the necessity of forming vacant, reduced  $\text{Mo}^{\text{IV}}$ .

Coordination of  $^3\text{O}_2$  to **11** to form the doublet peroxy species **13** has a calculated  $\Delta E = -32.2$  kcal/mol ( $\Delta G_{593K} = -8.3$  kcal/mol) (red curve in Figure 6). The distance of the shorter Mo–O bond in the  $\text{Mo}(\text{O}_2)$  peroxy moiety is 1.99 Å, indicating a bond order of almost 1 (0.08 Å longer than the bridging Mo–O bonds of the  $\text{Mo}_3\text{O}_9$  cluster). The longer Mo–O bond is 2.24 Å, where the lone pair on oxygen makes donor–acceptor coordination to the Mo. The O–O bond length of 1.34 Å indicates a bond order of 1.5 (compare to 1.33 Å for  $\text{HO}_2$  radical). The  $\langle S^2 \rangle$  value of **13** is 1.187, indicating a strong spin contamination from a quartet state that is 6.8 kcal/mol higher in energy than the corresponding doublet. The spin density is located in the  $d_{xz}$  orbitals of both reduced molybdenum sites and in the  $\text{OO}_\pi$  orbital that contributes a bond order of 0.5 to the 1.5 bond order of the O–O moiety.

The Mo–( $\text{O=CH-CH=CH}_2$ ) distance in **13** is 2.26 Å, which is 0.23 Å longer than in **11**, indicating a significantly weakened donor–acceptor coordination. Indeed the energy to remove the acrolein is reduced from 31.9 to 4.5 kcal/mol by chemisorbing the  $\text{O}_2$ .

We also located an isomer of species **13**, where one of the peroxy oxygens also coordinates to the *second* reduced Mo atom, with a Mo–O distance of 2.38 Å (**13'**). Isomer **13'** is significantly more stable than **13** (coordination  $\Delta E = -43.6$  kcal/mol,  $\Delta G = -15.5$  kcal/mol), most likely due to the energy gain from partially oxidizing both reduced Mo atoms. However, to accommodate this second coordination the Mo–Mo distance reduces from 3.60 to 3.31 Å, severely distorting the cluster structure. However, much like for the isomer of **12** described above, in a larger crystal we expect this distortion to be associated with a large energetic penalty, and we did not use this structure for further analysis.

Further discussions on the nature of bonding in such metal–peroxy systems and the relation to hydrocarbon oxidations was reported in the  $\text{V}_4\text{O}_{10}$ -catalyzed oxy dehydrogenation of propane to propene by Cheng et al.<sup>46</sup>

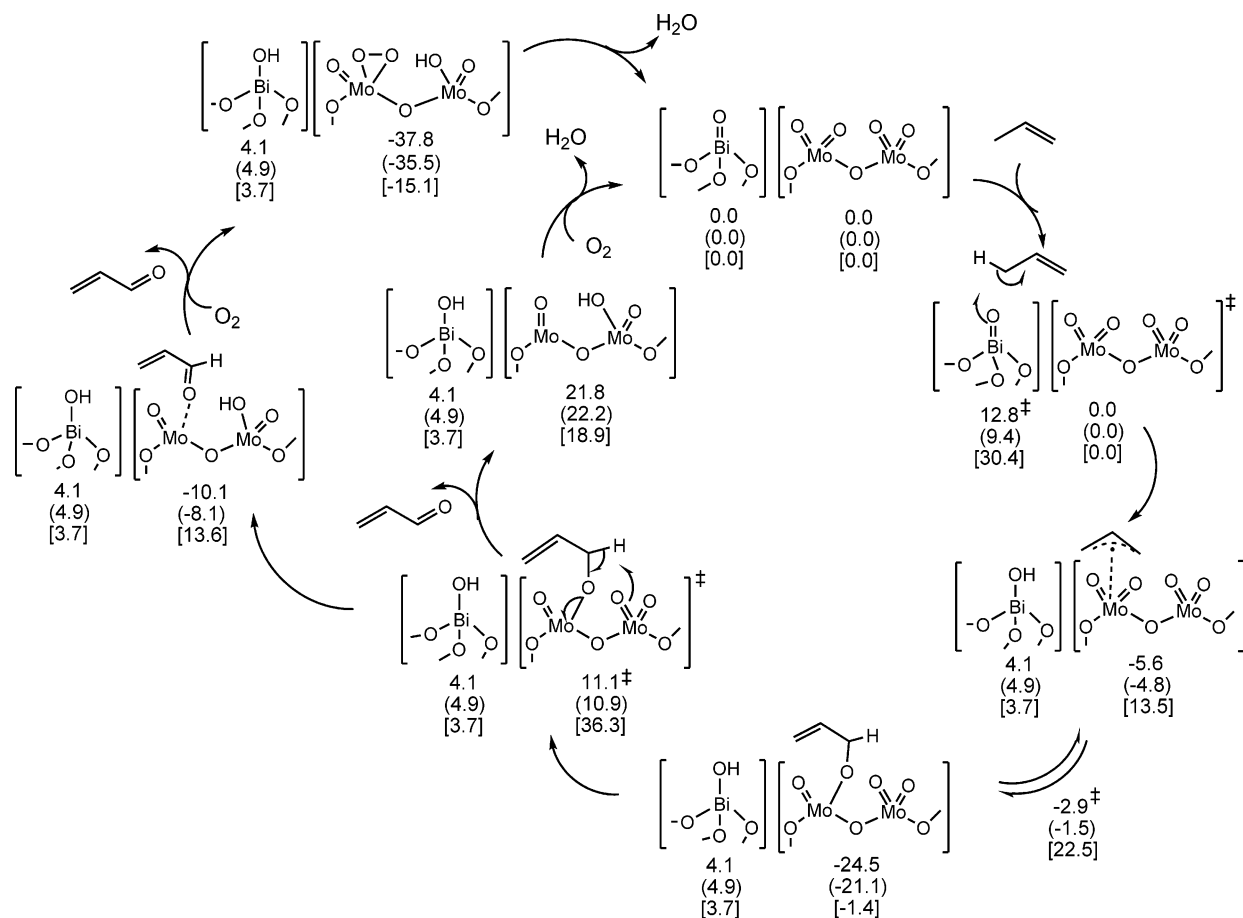
Desorption of acrolein from **13** is slightly endothermic on the  $\Delta E$  surface ( $\Delta E = 4.5$  kcal/mol) due to the weak coordination of acrolein to acidic molybdenum, although far less endothermic than from **11** ( $\Delta E = 31.9$  kcal/mol). However, on the free energy surface the desorption is now strongly exothermic ( $\Delta G_{593K} = -20.4$  kcal/mol), showing that reoxidizing the reduced sites prior to desorption significantly improves this process. Dissociating acrolein from **13** produces the cyclic peroxy  $\text{Mo}_3\text{O}_{10}\text{H}$  cluster **14**, which can be described as the product of a triplet  $\text{O}_2$  with a quartet state  $\text{Mo}_3\text{O}_8\text{H}$ . Both Mo–O bond distances in the Mo–( $\text{O}_2$ )ring are 1.93 Å, and the O–O bond distance is 1.46 Å, suggesting a single covalent O–O bond and two single covalent Mo–O bonds. The  $\langle S^2 \rangle$  value is 0.758, and there is no spin contamination in this species due to the absence of a  $\text{Mo}^{\text{IV}}$  center.

As mentioned above, it is generally assumed that migration of lattice oxygens is responsible for the reoxidation of the  $\text{Mo}^{\text{IV}}\text{--}(\text{O=CH-CH=CH}_2)$  and not molecular oxygen as in the above description. Nevertheless, these results indicate that acrolein can be desorbed easily from a surface site in the presence of available oxygens, either from the lattice or gas-phase  $\text{O}_2$ .

## 4. Discussion and Conclusions

**4.1. First CH Activation.** We calculate an activation enthalpy ( $\Delta H^\ddagger$ ) for the first hydrogen abstraction on the  $\text{Bi}^{\text{V}}$  site of the  $\text{Bi}_4\text{O}_7$  cluster to form an allyl radical of 11.0 kcal/mol ( $\Delta G_{593K}^\ddagger = 30.4$  kcal/mol), which is close to the measured  $\Delta H^\ddagger = 14$  kcal/mol for allyl radical formation on  $\text{Bi}_2\text{O}_3$ . We did not explore the barrier for CH activation on  $\text{Bi}^{\text{III}}$  sites, as we previously showed that the reaction  $\text{Bi}_4\text{O}_6 + \text{propene} \rightarrow \text{Bi}_4\text{O}_5(\text{OH}) + \text{allyl}$  is strongly endothermic ( $\Delta E = 50.9$  kcal/mol ( $\Delta G_{673K} = 41.6$  kcal/mol), and a barrier would thus be meaningless. However, we show here that propene activation on a  $\text{Mo}^{\text{VI}}$  site in a  $\text{Mo}_3\text{O}_9$  cluster (representing the  $\text{MoO}_3$  catalyst) has a barrier of 32.5 kcal/mol ( $\Delta G_{593K} = 48.1$  kcal/mol), which is in good agreement with the experimental observation that  $\text{MoO}_3$  is incapable of activating propene under conditions for which  $\text{Bi}_2\text{O}_3$  activates propene rapidly. Most likely, this is due to the stronger  $\text{Mo}^{\text{VI}}\text{=O}$  bond as compared to the  $\text{Bi}^{\text{V}}\text{=O}$  bond, and the absence of a driving force that would lower the activation energy (such as the formation of a  $\text{C=O}$  bond).

Although we know of no direct evidence from experiment of the role of  $\text{Bi}^{\text{V}}$ , the absence of alternative mechanisms and

SCHEME 2: Mechanism and Energetics for Propene Oxidation over Bismuth Molybdate<sup>a</sup>

<sup>a</sup> The top energy is the  $\Delta E$  from QM, the middle is  $\Delta H_{0K} = \Delta E + \Delta ZPE$ , and the bottom is  $\Delta G_{593K}$ . All reported values are in kcal/mol.

the agreement in the magnitude of the activation energy with experiment further supports the conclusion from theory that  $\text{Bi}^{\text{IV}}$  is involved. The lower value for the computed barriers as compared to the experimentally measured ones could be due to the relatively low concentration of  $\text{Bi}^{\text{IV}}$  sites on the catalyst surface, which would seemingly increase measured activation energy. Potentially, this could also explain the significantly different activation energies reported by other experimental investigations, as a change in experimental setup could influence the number of  $\text{Bi}^{\text{IV}}$  sites, which in turn would change the measured activation energy. This could be tested experimentally, either through testing on a surface with pregenerated  $\text{Bi}^{\text{IV}}$  sites, or through poisoning of potential  $\text{Bi}^{\text{IV}}$  sites on the regular  $\text{Bi}_2\text{O}_3$  surface.

**4.2. Allyl Adsorption.** We find that allyl chemisorption on  $\text{Bi}_2\text{O}_3$  is not favorable,  $\Delta E = 3.8$  kcal/mol ( $\Delta G_{593K} = 31.0$  kcal/mol),<sup>18</sup> whereas it is quite favorable on  $\text{MoO}_3$ ,  $\Delta E = -24.5$  kcal/mol ( $\Delta G_{593K} = -1.4$  kcal/mol), which is consistent with experiment. Most likely, the reason why it is not favorable on  $\text{Bi}_2\text{O}_3$  is the resulting reduction of  $\text{Bi}^{\text{III}}$  to the unfavorable  $\text{Bi}^{\text{II}}$  state, similar to the unfavorability of the initial CH activation step on  $\text{Bi}_2\text{O}_3$ . However, for the second step we cannot use the assumption that a  $\text{Bi}^{\text{IV}}$  site can do the required chemistry, as the odds of the activated allyl complex finding a *second*  $\text{Bi}^{\text{IV}}$  site should be very small, particularly compared to the probability of the allyl simply going back to propene. Thus, the chemisorption of the allyl on  $\text{MoO}_x$  is a requirement for further oxidation.

The  $\pi$ -allyl intermediate can rapidly convert to a  $\sigma$ -allyl intermediate (acrolein precursor) through the reversible forma-

tion of C–O bond, which is consistent with molecular probe experiments by Grasselli et al. (using D-labeled allyl alcohol over molybdate and bismuth molybdate catalysts).<sup>14,17</sup> Our calculations show that the conversion of  $\pi$ -allyl to  $\sigma$ -allyl is rapid, with a  $\Delta G_{593K}$  barrier of 9.0 kcal/mol, and the reverse process (i.e., the back-conversion of the  $\sigma$ -allyl to the  $\pi$ -allyl species) has a barrier of 23.9 kcal/mol. As such, this process is reversible under oxidation conditions, which agrees with the molecular probe experiments that show a rapid  $\pi$ -allyl  $\leftrightarrow$   $\sigma$ -allyl equilibrium. We compute  $k_{\text{H}}/k_{\text{D}} = 2.54$  for the second hydrogen abstraction which agrees with the experimental value of  $\approx 2.5$  at 320 °C. This, together with our observation that the second hydrogen abstraction is the rate-determining step for allyl conversion, explains the observed 70:30 ratio of acrolein-[3,3- $d_2$ ]:[1- $d_1$ ] produced from propene-[1,1- $d_2$ ] or propene-[3,3,3- $d_3$ ].

**4.3. Second CH Activation.** On  $\text{Mo}_3\text{O}_9$ , the net  $\Delta G_{593K}$  barrier for abstracting the second hydrogen to form acrolein is 37.7 kcal/mol. This is the rate-determining step in the conversion of  $\sigma$ -allyl intermediate to acrolein, in agreement with experiment. However, the magnitude of this barrier (37.7 kcal/mol) is too high for plausible reaction rates at 320 °C, and we conclude that pure  $\text{MoO}_3$  should not be an efficient catalyst for conversion of allyl to acrolein. This is also in good agreement with the experimental studies on allyl oxidation over pure  $\text{MoO}_3$ , which report acrolein yields of 0–51.5%, depending on the experimental conditions.

**4.4. Acrolein Desorption.** We found that desorption of acrolein to form a  $\text{Mo}^{\text{IV}}$  site is not favorable (endothermic by  $\Delta E = 31.9$  kcal/mol,  $\Delta G = 5.3$  kcal/mol), but we find that  $\text{O}_2$



can favorably assist desorption of acrolein. Binding  $O_2$  to the  $Mo^{IV}$ -acrolein complex is exothermic by  $\Delta E = -32.2$  kcal/mol ( $\Delta G = -8.3$  kcal/mol), leading to a stable  $Mo(acrolein)-(O_2)$  species from which the acrolein desorption energy is reduced to 4.5 kcal/mol ( $\Delta G = -20.4$  kcal/mol).

Next, we plan to examine the full pathway for propene oxidation on a model  $BiMoO_x$  mixed metal oxide cluster. Also, we are building these QM results into the ReaxFF reactive force fields<sup>48</sup> so that we can carry out molecular dynamics studies of these reactive processes on realistic mixed metal oxide surfaces.

## 5. Summary

The overall reaction mechanism, including both bismuth and molybdenum sites, is summarized in Scheme 2. We find a low-energy pathway for propene CH activation using  $Bi^V$  in  $Bi_4O_7$  cluster model, with a calculated barrier of  $\Delta E^\ddagger = 12.8$  kcal/mol ( $\Delta G^\ddagger = 30.4$  kcal/mol). This process is highly endothermic on  $Bi^{III}$ , whereas the pure molybdenum oxide exhibits a significantly higher barrier, suggesting that the CH activation event occurs on (relatively rare)  $Bi^V$  sites on the  $Bi_2O_3$  surface.

We studied the oxidation of allyl to acrolein over  $Mo_3O_9$ . This includes the adsorption of allyl to form the  $\pi$ -allyl and  $\sigma$ -allyl species, the second hydrogen abstraction, and dioxygen-assisted acrolein desorption. The absorption of allyl radical on  $Mo_3O_9$  is exothermic on the  $\Delta E$  surface, which helps offset a slight endothermicity of the allyl generation. The  $\pi$ -allyl complex can reversibly form a  $\sigma$ -allyl intermediate, with forward and reverse  $\Delta E^\ddagger$  ( $\Delta G^\ddagger$ ) barriers of 2.7 (9.0) kcal/mol and 21.6 (23.9) kcal/mol, respectively. The  $\sigma$ -allyl intermediate is significantly more stable than the  $\pi$ -allyl, with a relative energy of  $-24.5$  kcal/mol ( $\Delta G = -1.4$  kcal/mol). Acrolein is formed in a second hydrogen abstraction step from the  $\sigma$ -allyl intermediate and is the rate-determining step in this process with a calculated  $\Delta E^\ddagger = 35.6$  kcal/mol ( $\Delta G^\ddagger = 37.7$  kcal/mol). Finally, studies of acrolein desorption suggest that reoxidation of the reduced sites prior to acrolein desorption significantly improves this process.

**Acknowledgment.** The personnel involved in this research were partially supported by DOE (DE-PS36-03GO93015), ONR (N00014-06-1-0938), and Chevron. The facilities were supported by ARO-DURIP and ONR-DURIP funds.

**Supporting Information Available:** Computational details including Cartesian coordinates, energies, and vibrational frequencies. This material is available free of charge via the Internet at <http://pubs.acs.org>.

## References and Notes

- (1) Grasselli, R. K. *J. Chem. Educ.* **1986**, 63, 216.
- (2) Burrington, J. D.; Kartisek, C. T.; Grasselli, R. K. *J. Catal.* **1983**, 81, 489.
- (3) Grasselli, R. K.; Burrington, J. D.; Buttrey, D. J.; De Santo, P., Jr.; Lugmair, C. G.; Volpe, A. F., Jr.; Weingand, T. *Top. Catal.* **2003**, 23 (1–4), 5.
- (4) Burrington, J. D.; Grasselli, R. K. *J. Catal.* **1979**, 59, 79.
- (5) Massoth, F. E.; Scarpiello, D. J. *J. Catal.* **1971**, 21, 225.
- (6) Swift, H. E.; Bozik, J. E.; Ondrey, J. A. *J. Catal.* **1971**, 21, 212.
- (7) Grzybowska, B.; Haber, J.; Janas, J. *J. Catal.* **1977**, 49, 150.
- (8) Martir, W.; Lunsford, J. H. *J. Am. Chem. Soc.* **1981**, 103, 3728.
- (9) Adams, C. R.; Jennings, T. J. *J. Catal.* **1963**, 2, 63.
- (10) Adams, C. R.; Jennings, T. J. *J. Catal.* **1964**, 3, 549.
- (11) Voge, H. H.; Wagner, C. D.; Stevenson, D. P. *J. Catal.* **1963**, 2, 58.
- (12) Dozono, T.; Thomas, D. W.; Wise, H. *J. Chem. Soc., Faraday Trans. 1* **1973**, 69, 620.
- (13) White, M. G.; Hightower, J. W. *AIChE J.* **1981**, 27 (4), 545.
- (14) Burrington, J. D.; Kartisek, C. T.; Grasselli, R. K. *J. Catal.* **1980**, 63, 235.
- (15) Burrington, J. D.; Kartisek, C. T.; Grasselli, R. K. *J. Catal.* **1982**, 75, 225.
- (16) Burrington, J. D.; Kartisek, C. T.; Grasselli, R. K. *J. Catal.* **1984**, 87, 363.
- (17) Grasselli, R. K.; Burrington, J. D. *Ind. Eng. Chem. Prod. Res. Dev.* **1984**, 23, 393.
- (18) Jang, Y. H.; Goddard, W. A. *Top. Catal.* **2001**, 15, 273.
- (19) Jang, Y. H.; Goddard, W. A. *J. Phys. Chem. B* **2002**, 106, 5997.
- (20) DiCosimo, R.; Burrington, J. D.; Grasselli, R. K. *J. Catal.* **1986**, 102, 234.
- (21) Moro-Oka, Y.; Ueda, W. *Adv. Catal.* **1994**, 40, 233.
- (22) Allison, J. N.; Goddard, W. A. In *Active Sites on Molybdenum Surfaces, Mechanistic Considerations for Selective Oxidation and Ammoxidation of Propene*; Grasselli, R. K., Bradzil, J. F., Eds.; American Chemical Society: Washington, DC, 1985; Vol. 279, p 23.
- (23) Becke, A. D. *Phys. Rev. A* **1988**, 38, 3098.
- (24) Lee, C. T.; Yang, W. T.; Parr, R. G. *Phys. Rev. B* **1988**, 37, 785.
- (25) Hay, P. J.; Wadt, W. R. *J. Chem. Phys.* **1985**, 82, 299.
- (26) *Jaguar 6.5*; Schrodinger, LLC: Portland, OR, 2005.
- (27) Harwig, H. A. *Anorg. Allg. Chem.* **1987**, 444, 151.
- (28) France, M. R.; Buchanan, J. W.; Robinson, J. C.; Pullins, S. H.; Tucker, J. L.; King, R. B.; Duncan, M. A. *J. Phys. Chem. A* **1997**, 101, 6214.
- (29) Sidorov, L. N.; Minayeva, I. I.; Zasorin, E. Z.; Sorokin, I. D.; Borschevskiy, A. Y. *High Temp. Sci.* **1980**, 12, 175.
- (30) Oniyama, E.; Wahlbeck, P. G. *J. Phys. Chem. B* **1998**, 102, 4418.
- (31) Kienne, M.; Rademman, K. *Chem. Phys. Lett.* **1998**, 284, 363.
- (32) Fielicke, A.; Rademann, K. *J. Phys. Chem. A* **2000**, 104, 6979.
- (33) Bienati, M.; Bonacic-Koutecky, V.; Fantucci, P. *J. Phys. Chem. A* **2000**, 104, 6983.
- (34) Kihlborg, L. *Ark. Kemi* **1963**, 21, 357.
- (35) Van den Elzen, A. F.; Rieck, G. G. *Acta Crystallogr., Sect. B* **1973**, 29, 2433.
- (36) Berkowitz, J.; Inghram, M. G.; Chupka, W. A. *J. Chem. Phys.* **1957**, 26, 842.
- (37) Fialko, E. F.; Kikhtenko, A. V.; Goncharov, V. B.; Zamazaev, K. I. *J. Phys. Chem. A* **1997**, 101, 8607.
- (38) Fialko, E. F.; Kikhtenko, A. V.; Goncharov, V. B. *Organometallics* **1998**, 17, 25.
- (39) Fu, G.; Xu, X.; Lu, X.; Wan, H. *J. Am. Chem. Soc.* **2005**, 127, 3989.
- (40) Fu, G.; Xu, X.; Lu, X.; Wan, H. *J. Phys. Chem. B* **2005**, 109, 6416.
- (41) Matsuura, I. *J. Catal.* **1974**, 33, 240.
- (42) Rappe, A. K.; Goddard, W. A. *J. Am. Chem. Soc.* **1982**, 104, 3287.
- (43) Keulk, G. W. *J. Catal.* **1970**, 19, 232.
- (44) Krenzke, L. D.; Keulks, G. W. *J. Catal.* **1980**, 61, 316.
- (45) Glaeser, L. C.; Brazdil, J. F.; Hazel, M. A. S.; Meheciec, M.; Grasselli, R. K. *J. Chem. Soc., Faraday Trans.* **1985**, 81, 2903.
- (46) Cheng, M.; Chenoweth, K.; Oxgaard, J.; van Duin, A.; Goddard, W. A. *J. Phys. Chem. C* **2007**, 111, 5115.
- (47) Chempath, S.; Bell, A. T. *J. Catal.* **2007**, 247, 119.
- (48) Goddard, W. A., III; van Duin, A.; Chenoweth, K.; Cheng, M.; Pudar, S.; Oxgaard, J.; Merinov, B.; Jang, Y. H.; Persson, P. *Top. Catal.* **2006**, 38, 93.